J|A|C|S ARTICLES

Published on Web 03/10/2009

Spin Dynamics in the Negatively Charged Terbium (III) Bis-phthalocyaninato Complex

Francesca Branzoli,[¶] Pietro Carretta,*[,¶] Marta Filibian,[¶] Giorgio Zoppellaro,[‡,†] Michael J. Graf,[||] Jose R. Galan-Mascaros,[$] Olaf Fuhr,[‡] Susan Brink,[‡] and Mario Ruben*[,‡]

Department of Physics "A.Volta", University of Pavia-CNISM, Via Bassi 6, I-27100 Pavia, Italy, Department of Physics, Boston College, Chestnut Hill, Massachusetts 02467, Institute of Nanotechnology, Karlsruhe Institute of Technology (KIT), Hermann-von-Helmholtz-Platz 1, 76344 Eggenstein-Leopoldshafen, Germany, Instituto de Ciencia Molecular (ICMOL), Universidad de Valencia, Polígono de la Coma, s/n, 46980 Paterna, Spain, and Department of Molecular Biosciences, University of Oslo, N-0316 Oslo, Norway

Received November 4, 2008; E-mail: mario.ruben@int.fzk.de; carretta@fisicavolta.unipv.it

Abstract: The experimental and theoretical study of the electron spin dynamics in the anionic form of a single-ion molecule magnet (SIMM), the bis-phthalocyaninato terbium (III) molecule $[Pc_2Tb]^-[TBA]^+$, has been addressed by means of solid state ^1H NMR spectroscopy. The magnetic properties of the caged Tb^{3+} metal center were investigated in a series of diamagnetically diluted preparations, where the excess of tetrabutylamonium bromide $([TBA]Br)_n$ salt was used as diamagnetic matrix complement. We found that a high temperature activated spin dynamics characterizes the systems, which involved phonon-assisted transitions among the crystal field levels in qualitative agreements with literature results. However, the activation barriers in these processes range from 641 cm^{-1} for the diamagnetically diluted samples to 584 cm^{-1} for those undiluted; thus, they exhibit barriers 2−3 times larger than witnessed in earlier (230 cm^{-1}) reports (e.g., Ishikawa, N.; Sugita, M.; Ishikawa, T.; Koshihara, S.; Kaizu, Y. *J. Am. Chem. Soc.* **2003**, *125*, 8694−8695). At cryogenic temperatures, fluctuations are driven by tunneling processes between the $m = +6$ and -6 low-energy levels. We found that the barrier Δ and the tunneling rates change from sample to sample and especially the diamagnetically diluted $[Pc_2Tb]^-$ molecules appear affected by the sample's magneto/thermal history. These observations emphasize that matrix arrangements around $[Pc_2Tb]^-$ can appreciably alter the splitting of the crystal field levels, its symmetry, and hence, the spin dynamics. Therefore, understanding how small differences in molecular surroundings (as for instance occurring by depositing on surfaces) can trigger substantial modifications in the SIMM property is of utmost importance for the effective operation of such molecules for single-molecule data storage, for example.

Introduction

The correlation between the magnetic and structural properties of metallic and hybrid (metallo-organic)-based materials has fascinated chemist, physicist, and theoretical chemist due to the rich variety of phenomena that such materials exhibit, providing inspiration for their potential application in materials science.[1] By far, the most important class of magnetic compounds for practical applications belongs to the group of ferromagnets.[2,3] In these materials the unpaired spins spontaneously align parallel to each other in macroscopic domains, and permanent net-magnetization can be obtained under appropriate conditions. About two decades ago the discovery that some polynuclear metallo-organic complexes possessing high-spin multiplicity (S_T) combined with large negative zero-field-splitting (D) can behave as classical superparamagnets promoted formidable research synergy among synthetic, materials chemists and physicists.[4] In these systems the size of the magnetic domains is scaled down to the single-molecule level and provides ground to correlate phenomena that span from the nanoscopic to the microscopic world. Molecules exhibiting superparamagnetic properties show, in addition, staircase-like magnetization hysteretic loops, where the step substructure arises from the presence of quantum-tunneling paths in the magnetization

[¶] University of Pavia-CNISM.
[||] Boston College.
[‡] Institute of Nanotechnology, Karlsruhe Institute of Technology (KIT).
[$] Universidad de Valencia.
[†] University of Oslo.

(1) Coronado, E.; Day, P. *Chem. Rev.* **2004**, *104*, 5419–5448.
(2) Gatteschi, D., Kahn, O., Miller, J. S., Palacio, F., Eds. *Magnetic Molecular Materials*; NATO ASI Series 198, Kluwer Academic Publishers: Dordrecht, 1991.
(3) Kahn, O. *Molecular Magnetism*; Wiley-VCH Inc.: New York, 1993.
(4) (a) Miller, J. S., Drillon, M., Eds. *Magnetism: Molecules to Materials*; Wiley-VCH Verlag: Weinheim, 2001; Vol. I, Models and Experiments. (b) Miller, J. S., Drillon, M., Eds. *Magnetism: Molecules to Materials*; Wiley-VCH Verlag: Weinheim, 2001; Vol. II, Molecule-Based Materials. (c) Miller, J. S., Drillon, M., Eds. *Magnetism: Molecules to Materials*; Wiley-VCH Verlag: Weinheim, 2002; Vol. III, Nanosized Magnetic Materials. (d) Miller, J. S., Drillon, M., Eds. *Magnetism: Molecules to Materials*; Wiley-VCH Verlag: Weinheim, 2003; Vol. IV. (e) Miller, J. S., Drillon, M., Eds. *Magnetism: Molecules to Materials*; Wiley-VCH Verlag: Weinheim, 2005; Vol. V.

between levels on the double-well potential system model.[5−7] Combination of these fingerprints together with the presence of phenomena such as quantum phase interference[8] has been used to classify these systems as single-molecule magnets (SMMs).[9] The research efforts in the field are directed toward better understanding of the quantum nature of SMM compounds which should gate their synthetic design.[10] Several metallo-organic complexes behaving like SMMs have been discovered in recent years and include, for example, the well-known family of Mn_{12} cluster complexes and derivatives,[11−19] polynuclear iron complexes,[20] and distorted cubane synthons,[21−25] In SMMs the slow relaxation of the magnetization arises from the uniaxial anisotropy D of the molecule, which brings at low temperature the direction of the molecular magnetization vector **M** to be fixed and leads to suppression of spin reversal. In this scenario the relaxation time (τ) of **M** obeys the thermally activated Arrhenius law, which is expressed as:

$$\tau(T) = \tau_0 \exp(\Delta/k_bT)$$

Here, the energy barrier for the magnetization reversal, Δ, is described by $|D|S_T^2$ for integer S_T and $|D|(S_T^2 - 1/4)$ for half-integer S_T.[6,26] Since the properties of SMMs are to a certain degree[27−31] defined mainly by the intrinsic nature of the individual molecule parameters (S_T and D), the resulting large, bistable spin anisotropy can deliver, in principle, the smallest practical unit for assembling molecular spintronic elements[32] such as magnetic memory devices and the achievement of quantum computing.[33,34] The technological prospect for an authentic use of molecules in these fields found ground recently in the experimental observation of Rabi oscillations in the $[V_{15}^{IV}As_6^{III}O_{42}(H_2O)]^{6-}$ cluster anion.[35] However, limits on practical application can be easily foreseen, since their operational working temperatures are dictated by the blocking temperature T_b of the SMM molecule. The preparation of SMM metal complexes represents yet a synthetic challenge;[36] the arrangement of the Jahn−Teller axes of metal ions by bridging ligands must be engineered in a fashion that brings both high-spin ground-state and large negative zero-field splitting ($D \geq -0.1$ cm^{-1}). To date, the record magnetization reported in multimetal cluster SMMs belongs to the manganese compound $[Mn^{III}_6O_2(Etsao)_6\{O_2CPh(Me)_2\}(EtOH)_6]$, where $Etsao^{2-}$ derives from $EtsaoH_2$ which indicates 2-hydroxyphenylpropanone oxime and $(Me)_2PhCO_2^-$ stands for 3,5-dimethylbenzoate.[37] The complex showed high-spin ground state, $S = 12$, quite large axial anisotropy, $D = -0.43$ cm^{-1}, thermal barrier Δ for spin-flipping of 86.4 K, $\tau_0 = 2 \times 10^{-10}$ s, and blocking temperature T_b of around 4.3 K. These properties slightly improved those found earlier in the $[Mn_{12}O_{12}(O_2CR)_{16}(H_2O)_4]$ (R = various groups) family, with $S = 10$ ground state, $T_b \approx 3.5$ K, and $\Delta \leq 74$ K.[38] A different class of SMMs emerged recently[39] where slow relaxation of the magnetic moment arises from a single *f*-metal ion coordinated by the isoindoline nitrogens of two phthalocyaninato (*Pc*) rings. These compounds are formulated in literature as Pc_2M.[40,41] The discovery of slow magnetization relaxation, hysteretic behavior, and also resonant quantum tunneling between hyperfine levels appears as a characteristic of rare-earth metal ions. Such properties were discussed in literature just a few years ago, through experimental and

(5) Thomas, L.; Lionti, F.; Ballau, R.; Gatteschi, D.; Sessoli, R.; Barbara, B. *Nature* **1996**, *383*, 145–147.
(6) Gatteschi, D.; Sessoli, R. *Angew. Chem., Int. Ed.* **2003**, *42*, 268–297.
(7) Friedman, J. R.; Sarachick, M. P.; Tejada, J.; Ziolo, R. *Phys. Rev. Lett.* **1996**, *76*, 3830–3833.
(8) Wernsdorfer, W.; Sessoli, R. *Science* **1999**, *284*, 133–135.
(9) Christou, G.; Gatteschi, D.; Hendrichson, D. N.; Sessoli, R. *MRS Bull.* **2000**, *25*, 66–71.
(10) Aromi, G.; Aubin, S. M. J.; Bolcar, M. A.; Christou, G.; Eppley, H. J.; Folfting, K.; Hendrickson, D. N.; Huffman, J. C.; Squire, R. C.; Tsai, H.-L.; Wang, S.; Wemple, M. W. *Polyhedron* **1998**, *17*, 3005–3020.
(11) Lis, T. *Acta Crystallogr.* **1980**, *B36*, 2042–2046.
(12) Sessoli, R.; Tsai, H.-L.; Schake, A. R.; Wang, S.; Vincent, J. B.; Folting, K.; Gatteschi, D.; Christou, G.; Hendrickson, D. N. *J. Am. Chem. Soc.* **1993**, *115*, 1804–1816.
(13) Sessoli, R.; Gatteschi, D.; Caneschi, A.; Novak, M. A. *Nature* **1993**, *365*, 141–143.
(14) Eppley, H. J.; Tsai, H.-L.; de Vries, N.; Folting, K.; Christou, G.; Hendrickson, D. N *J. Am. Chem. Soc.* **1995**, *117*, 301–317.
(15) Aubin, S. M. J.; Sun, Z.; Pardi, L.; Krzystek, J.; Folting, K.; Brunel, L.-C.; Rheingold, A. L.; Christou, G.; Hendrickson, D. N. *Inorg. Chem.* **1999**, *38*, 5329–5340.
(16) Boskovic, C.; Pink, M.; Huffman, J. C.; Hendrickson, D. N.; Christou, G. *J. Am. Chem. Soc.* **2001**, *123*, 9914–9915.
(17) Soler, M.; Chandra, S. K.; Ruiz, D.; Davidson, E. R.; Hendrickson, D. N.; Christou, G. *Chem. Commun.* **2000**, *24*, 2417–2418.
(18) Brechin, E. K.; Boskovic, C.; Wernsdorfer, W.; Yoo, J.; Yamaguchi, A.; Sanudo, E. C.; Concolino, T. R.; Rheingold, A. L.; Ishimoto, H.; Hendrickson, D. N.; Christou, G. *J. Am. Chem. Soc.* **2002**, *124*, 9710–9711.
(19) Soler, M.; Wernsdorfer, W.; Folting, K.; Pink, M.; Christou, G. *J. Am. Chem. Soc.* **2004**, *126*, 2156–2165.
(20) Sangregorio, C.; Ohm, T.; Paulsen, C.; Sessoli, R.; Gatteschi, D. *Phys. Rev. Lett.* **1997**, *78*, 4645–4648.
(21) Aubin, S. M. J.; Wemple, M. W.; Adams, D. M.; Tsai, H.-L.; Christou, G.; Hendrickson, D. N. *J. Am. Chem. Soc.* **1996**, *11*, 7746–7754.
(22) (a) Aubin, S. M. J.; Dilley, N. R.; Pardi, L.; Krzystek, J.; Wemple, M. W.; Brunel, L. C.; Maple, M. B.; Christou, G.; Hendrickson, D. N. *J. Am. Chem. Soc.* **1998**, *120*, 4991–5004. (b) Aubin, S. M. J.; Dilley, N. R.; Wemple, M. W.; Maple, M. B.; Christou, G.; Hendrickson, D. N. *J. Am. Chem. Soc.* **1998**, *120*, 839–840.
(23) Andres, H.; Basler, R.; Gudel, H.-U.; Aromi, G.; Christou, G.; Buttner, H.; Ruffle, B. *J. Am. Chem. Soc.* **2000**, *122*, 12469–12477.
(24) (a) Schelter, E. J.; Karadas, F.; Avendano, C.; Prosvirin, A. V.; Wernsdorfer, W.; Dunbar, K. R. *J. Am. Chem. Soc.* **2007**, *129*, 8139–8149. (b) Muller, A.; Peters, F.; Pope, M. T.; Gatteschi, D. *Chem. Rev.* **1998**, *98*, 239–271.
(25) Castro, S. L.; Sun, Z.; Grant, C. M.; Bollinger, J. C.; Hendrickson, D. N.; Christou, G. *J. Am. Chem. Soc.* **1998**, *120*, 2365–2375.
(26) Gatteschi, D.; Sessoli, R.; Villain, J. *Molecular Nanomagnets*; Oxford University Press; New York, 2006.
(27) Goodwin, J. C.; Sessoli, R.; Gatteschi, D.; Wernsdorfer, W.; Powell, A. K.; Heath, S. L. *J. Chem. Soc., Dalton Trans.* **2000**, *12*, 1835–1840.
(28) Boskovic, C.; Bircher, R.; Tregenna-Piggott, P. L. W.; Güdel, H. U.; Paulsen, C.; Wernsdorfer, W.; Barra, A.-L.; Khatsko, E.; Neels, A.; Stoeckli-Evans, H. *J. Am. Chem. Soc.* **2003**, *125*, 14046–14058.
(29) Wernsdorfer, W.; Aliaga-Alcalde, N.; Hendrickson, D. N.; Christou, G. *Nature* **2002**, *416*, 406–409.
(30) Tiron, R.; Wernsdorfer, W.; Foguet-Albiol, D.; Aliaga-Alcalde, N.; Christou, G. *Phys. Rev. Lett.* **2003**, *91*, 227203.
(31) Miyasaka, H.; Yamashita, M. *Dalton Trans.* **2007**, 399–406.
(32) Bogani, L.; Wernsdorfer, W. *Nat. Mater.* **2008**, *7*, 179–186.
(33) DiVincenzo, D. P. *Science* **1995**, *270*, 255–261.
(34) (a) Leuenberger, M. N.; Loss, D. *Nature* **2001**, *410*, 789–793. (b) Affronte, M.; Troiani, F.; Ghirri, A.; Candini, A.; Evangelisti, M.; Corradini, V.; Santini, P.; Amoretti, G.; Tuna, G.; Winpenny, R. E. P. *J. Phys. D: Appl. Phys.* **2007**, *40*, 2999–3004. (c) Wernsdorfer, W. *Nat. Mater.* **2007**, *6*, 174–176.
(35) Bertaina, S.; Gambarelli, S.; Mitra, T.; Tsukerblat, B.; Müller, A.; Barbara, B. *Nature* **2008**, *453*, 203–206.
(36) Aromi, G.; Claude, J.-P.; Knapp, M. J.; Huffman, J. C.; Hendrickson, D. N.; Christou, G. *J. Am. Chem. Soc.* **1998**, *120*, 2977–2978.
(37) Milios, C. J.; Vinslava, A.; Wernsdorfer, W.; Moggach, S.; Parsons, S.; Perlepes, S. P.; Christou, G.; Brechin, E. K. *J. Am. Chem. Soc.* **2007**, *129*, 2754–2755.
(38) Chakov, N. E.; Lee, S.-C.; Harter, A. G.; Kuhns, P. L.; Reyes, A. P.; Hill, S. O.; Dalal, N. S.; Wernsdorfer, W.; Abboud, K.; Christou, G. *J. Am. Chem. Soc.* **2006**, *128*, 6975–6989.
(39) Ishikawa, N.; Sugita, M.; Ishikawa, T.; Koshihara, S.; Kaizu, Y. *J. Am. Chem. Soc.* **2003**, *125*, 8694–8695.
(40) Ishikawa, N.; Sugita, M.; Ishikawa, T.; Koshihara, S.; Kaizu, Y. *J. Phys. Chem. B* **2004**, *108*, 11265–11271.
(41) Ishikawa, N.; Sugita, M.; Wernsdorfer, W. *J. Am. Chem. Soc.* **2005**, *127*, 3650–3651.

theoretical analyses of the magnetic behavior of $LiY_{0.998}Ho_{0.002}F_4$, a prototype of a diluted single-ion magnet.[42] On the other hand, the synthesis of Pc_2M synthons is dated from the 1960s,[43−45] and those studies were complemented years later by the investigation of the magnetic properties.[46−48] The structural information available for some Pc_2M molecules provides evidence that the caged *f*-block metal (III) ions adopt, as expected, eight-fold coordination motifs.[46,49−53] Pc_2Ms can exist in different forms, based on the oxidation state of the *Pc* rings.[46,48,49,54,55] The anionic form, indicated hereafter with the general formula $[Pc_2M]^-$, consists of a trivalent lanthanide ion (+3) coordinated by two *Pc* ligands, each one bearing a formal charge of −2. Here, the organic core adopts a closed shell π-electronic configuration. The resulting negative charge located on $[Pc_2M]^-$ needs to be stabilized by a countercation, such as the commonly used bulky *n*-tetrabutylammonium $[TBA]^+$ molecule. The neutral species $[Pc_2M]^0$ corresponds to one electron oxidation form which occurs on the ligand side of the complex. In this case, the organic core features the open shell π-electronic configuration. Ishikawa and co-workers first, followed later on by joint works with Wernsdorfer, demonstrated that the anionic complexes $[Pc_2Tb]^-[TBA]^+$, $[Pc_2Dy]^-[TBA]^+$, and $[Pc_2Ho]^-[TBA]^+$ possess signatures of single-ion molecular magnets (SIMM); hence, they exhibit slow magnetization relaxation as single-molecular property, hysteretic behaviors around 2 K (Tb, Dy) and 0.5 K (Ho), and resonant quantum tunneling of magnetization between hyperfine levels.[38−40,56,57] In particular, $[Pc_2Tb]^-[TBA]^+$ showed out-of-phase frequency-dependent AC susceptibility (χ'') peaks at 40 K, a temperature considerably higher than those observed for the SMMs with caged *d*-block transition metals. In these systems, the relaxation processes of the lanthanide ions arise from the energy exchange between the *f*-metals and phonon-assisted radiations. The effective energy barrier Δ for the magnetic moment reversal is thus determined by the ligand field potential (CF) around the *f*-metal, which partially relieves the degeneracy in J_z for the ground state. In $[Pc_2Tb]^-[TBA]^+$, the lowest substates with J_z eigenvalue $m = \pm 6$ are separated from the second-lowest $m = \pm 5$ states by a large energy gap ≈ 400 cm^{-1}.[57] Such electronic configuration strongly hinders the transition probability between the lowest substates. The energy sublevel structures of the ground-state multiplets were obtained through combination of high resolution ^{1}H NMR shifts (in solution) and bulk magnetic susceptibility measurements.[40,58] Accordingly, two different temperature-dependent relaxation processes were suggested to characterize $[Pc_2Tb]^-[TBA]^+$: (i) the two-phonon Orbach process, which is dominant in the range 25 K $\leq T \leq$ 40 K and (ii) the Raman scattering that becomes active below 25 K. In this work we analyze the spin dynamics of the $[Pc_2Tb]^-$ complex in a series of different diamagnetically diluted preparations, $[Pc_2Tb]^-[TBA]^+$ (**1**), $[Pc_2Tb]^-[TBA]^+ \times 9$ [TBA]Br (**2**), and $[Pc_2Tb]^-[TBA]^+ \times 143$ [TBA]Br (**3**), using tetrabutylamonium bromide as matrix $([TBA]Br)_n$ complement. The use of $[TBA]^+$ brings, in addition to its bulkiness, the positive charge necessary to balance the negative charge located on the $[Pc_2Tb]^-$complex and guarantees its prolonged stability over time. The experiments were performed with the aid of solid-state ^{1}H NMR spectroscopy, a technique that successfully described the spin relaxation behavior in Mn_{12} cluster.[59] From the temperature dependence of the spin−lattice relaxation rate, $1/T_1$, the characteristic correlation time for Tb^{3+} moment fluctuations has been derived for the very diluted samples, $[Pc_2Tb]^-[TBA]^+ \times 143$ [TBA]Br (**3**) and $[Pc_2Tb]^-[TBA]^+ \times 9$ [TBA]Br (**2**), as well as for the undiluted $[Pc_2Tb]^-[TBA]^+$ (**1**) samples. High temperature activated spin dynamics, involving phonon-assisted transitions among the crystal field levels, have been confirmed in qualitative agreement with previous results.[40] However, the activation barriers in the processes range from 923 K for the more diluted samples **2** and **3** to about 840 K for the undiluted $[Pc_2Tb]^-[TBA]^+$ (**1**) molecule; such values are much larger than those reported earlier in the $[Pc_2Tb]^-[TBA]^+$ system.[40] At low temperatures, fluctuations are driven by tunneling processes between the $m = +6$ and -6 low-energy levels. We found that the energy barrier Δ and the tunneling rate changed from sample to sample and appeared to be affected by their magneto/thermal history. These observations emphasize that even the diamagnetic [TBA]Br matrix arrangement around the $[Pc_2Tb]^-$ complexes can alter the splitting of the crystal field levels, and hence the Tb^{3+} spin dynamics. Understanding how small differences in molecular surrounding can trigger substantial modifications of the SIMM property is of utmost importance for ongoing research on surface-deposited bis-phthalocyaninato terbium (III) molecules targeting the realization of single molecular data storage.[60−62]

Results and Discussion

Synthesis of $[Pc_2Tb]^-[TBA]^+$ and Its Spectroscopic Characterization. The synthesis of Pc_2M synthons relies mostly on templating reactions, starting from the phthalonitrile precursor, in the presence of a strong base (e.g., DBU, alkoxides) and high-

(42) (a) Giraud, R.; Wernsdorfer, W.; Tkachuk, A.; Mailly, D.; Barbara, B. *Phys. Rev. Lett.* **2001**, *87*, 057203. (b) Giraud, R.; Tkachuk, A. M.; Barbara, B. *Phys. Rev. Lett.* **2003**, *91*, 257204.
(43) Kirinp, I. S.; Moskalev, P. N.; Makashev, Y. A. *Russ. J. Inorg. Chem.* **1965**, *10*, 1065–1066.
(44) Kirinp, I. S.; Moskalev, P. N.; Makashev, Y. A. *Russ. J. Inorg. Chem.* **1967**, *12*, 369–372.
(45) Kirin, I. S.; Shelekhi, Y. L.; Moskalev, Y. A. *Sov. Phys. Solid State (Engl. Transl.)* **1967**, *9*, 1461.
(46) Decian, A.; Moussavi, M.; Fischer, J.; Weiss, R. *Inorg. Chem.* **1985**, *24*, 3162–3167.
(47) Trojan, K. L.; Hatfield, W. E.; Kepler, K. D.; Kirk, M. L. *J. Appl. Phys.* **1991**, *69*, 6007–6009.
(48) Trojan, K. L.; Kendall, J. L.; Kepler, K. D.; Hatfield, W. E. *Inorg. Chim. Acta* **1992**, *198*, 795–803.
(49) Moussavi, M.; De Cian, A.; Fischer, J.; Weiss, R. *Inorg. Chem.* **1988**, *27*, 1287–1291.
(50) Haghighi, M. S.; Teske, Ch. R. L.; Honborg, H. *Z. Anorg. Allg. Chem.* **1992**, *608*, 73–80.
(51) Koike, N.; Uekusa, H.; Ohashi, Y.; Harnoode, C.; Kitamura, F.; Ohsaka, T.; Tokuda, K. *Inorg. Chem.* **1996**, *35*, 5798–5804.
(52) Kasuga, K.; Tsutsui, M.; Petterson, R. C.; Tatsumi, K.; Van Opdenbosch, N.; Pepe, G.; Meyer, E. F. *J. Am. Chem. Soc.* **1980**, *102*, 4835–4836.
(53) Loosli, C.; Liu, S.-X.; Neels, A.; Labat, G.; Decurtins, S. *Z. Kristallogr.* **2006**, *221*, 135–141.
(54) Konami, H.; Hatano, M.; Kobayashi, N.; Osa, T. *Chem. Phys. Lett.* **1990**, *165*, 397–400.
(55) Harnoode, C.; Takamura, K.; Kubota, H.; Sho, K.; Fujisawa, K.; Kitamura, F.; Ohsaka, T.; Tokuda, K. *Electrochemistry* **1999**, *67*, 832–838.
(56) Ishikawa, N.; Sugita, M.; Wernsdorfer, W. *Angew. Chem., Int. Ed.* **2005**, *44*, 2931–2935.
(57) Ishikawa, N. *Polyhedron* **2007**, *26*, 2147–2153.
(58) Ishikawa, N.; Sugita, M.; Okubo, T.; Tanaka, N.; Iino, T.; Kaizu, Y. *Inorg. Chem.* **2003**, *42*, 2440–2446.
(59) Lascialfari, A.; Jang, Z. H.; Borsa, F.; Carretta, P.; Gatteschi, D. *Phys. Rev. Lett.* **1998**, *81*, 3773–3776.
(60) Vitali, L.; Fabris, S.; Mosca Conte, A.; Brink, S.; Ruben, M.; Baroni, S.; Kern, K. *Nano Lett.* **2008**, *8*, 3364–3368.
(61) Osorio, E.; Bjornholm, T.; Lehn, J.-M.; Ruben, M.; van der Zant, H. S. J. *J. Phys.: Condens. Matter* **2008**, *20*, 374121–374131.
(62) Ruben, M.; Landa, A.; Lörtscher, E.; Riel, H.; Mayor, M.; Görls, H.; Weber, H. B.; Arnold, A.; Evers, V. *Small* **2008**, *12*, 2229–2235.

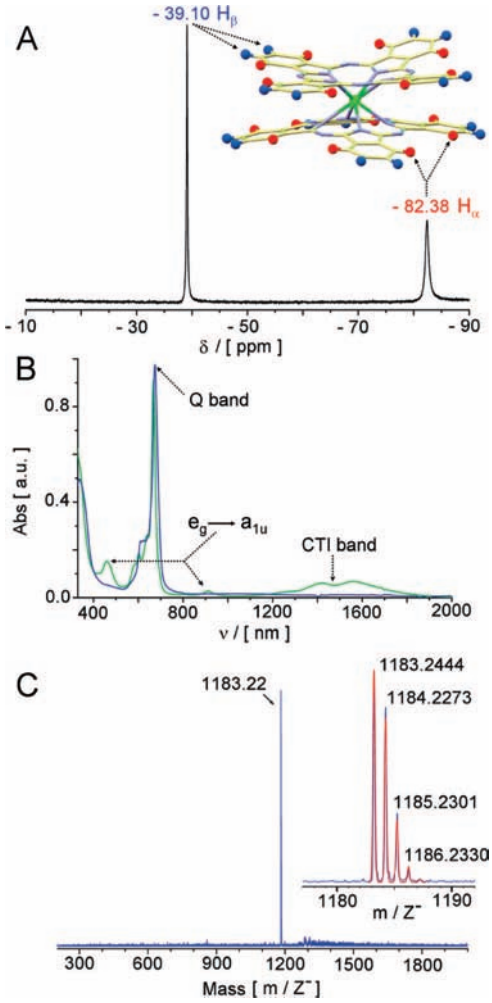

Figure 1. (A) ^{1}H NMR spectrum of $[Pc_2Tb]^-[TBA]^+$ (**1**) recorded in CD_3CN showing the chemical shifts for the H_α and H_β protons of the phthalocyanine rings. (B) UV/vis/nIR (MeOH) of $[Pc_2Tb]^-[TBA]^+$ (**1**) (blue line). The neutral form $[Pc_2Tb]^0$ (green line) is shown for comparison. (C) Maldi-ToF mass spectrum of $[Pc_2Tb]^-[TBA]^+$ (**1**) with the molecular peak of $[Pc_2Tb]^-$ ($m/z^- = 1183.22$, 100%, M^-) recorded in the negative polarity mode. The small inset shows the high-resolution Maldi-ToF peak of $[Pc_2Tb]^-$ evidencing the isotopic distribution pattern (blue line) together with its simulation (red line).

boiling solvents, such as pentanol or hexanol. The molecular assembly of $[Pc_2Tb]^-[TBA]^+$ was carried out throughout this work by employing microwave energy, as an alternative to conventional heating. In this way, side reactions and especially formation of large amounts of empty phthalocyanine rings appeared hindered. Both forms, the anionic, $[Pc_2Tb]^-$, and neutral, $[Pc_2Tb]^0$, were obtained simultaneously, as observed in other earlier reports,[46−49] but their relative ratio, which strongly depends on heating gradients, allowed mostly formation of the negative form $[Pc_2Tb]^-$ because of the fast thermal gradients induced through microwave heating. Purification of the negatively charged complex was very demanding, and is reported in detail in the Experimental Section. The stabilization of the anionic form $[Pc_2Tb]^-$ was obtained by stoichiometric addition of *n*-tetrabutylamonium bromide salt [TBA]Br while excess of salt has been used for the diamagnetically diluted preparations, $[Pc_2Tb]^-[TBA]^+ \times 143$ [TBA]Br (**3**) and $[Pc_2Tb]^-[TBA]^+ \times 9$ [TBA]Br (**2**). The paramagnetic ^{1}H NMR spectrum of $[Pc_2Tb]^-[TBA]^+$ (**1**) in solution is presented in Figure 1A. The experimentally observed dipolar shifts for α-protons (− 82.38 δ/ppm, H_α) and β-protons (− 39.10 δ/ppm, H_β) of the phthalocyanine cores were well resolved in CD_3CN, in close agreement with previous findings (− 85.4 δ/ppm for H_α, − 40.58 δ/ppm H_β)[58] and such shifts in solution were not effected by further addition (excess) of [TBA]Br, as it occurs in **2** and **3**. The UV/vis/nIR absorption spectrum (MeOH) of $[Pc_2Tb]^-[TBA]^+$ is shown in Figure 1B. It exhibits Soret (336 nm) and Q-bands (674 nm) at the expected positions, while the $e_g \rightarrow a_{1u}$ transitions (460 and 910 nm) and the CTI transitions (charge transfer intervalence band, above 1400 nm) are clearly missing. Those signals (CTI and $e_g \rightarrow a_{1u}$) are known to represent fingerprints of the neutral specie $[Pc_2Tb]^0$, and thus confirm the absence of contamination derived from the neutral $[Pc_2Tb]^0$ form in the $[Pc_2Tb]^-[TBA]^+$ compound.[45] The Maldi-ToF mass spectrum of $[Pc_2Tb]^-[TBA]^+$ (**1**) (Figure 1C) showed clearly the molecular peak for $[Pc_2Tb]^-$ ($m/z^- = 1183.22$, 100%, M^-) only when negative polarity mode was applied within the acquisition procedure, while the cationic part $[TBA]^+$ ($m/z^+ = 241.87$, 100%, M^+) could be detected only in positive polarity (see Supporting Information), as indication of their respective charges.

Single Crystal X-ray Analysis of $[Pc_2Tb]^-[TBA]^+ \times 3$ $[TBA]^+Br^- \times 3$ H_2O (4). Starting from the diluted $[Pc_2Tb]^-[TBA]^+ \times 9$ [TBA]Br sample, the molecular complex (**4**) crystallized in MeOH, forming blue-violet needles, within few days. In fact, the single-crystal analysis resulted in the composition $[Pc_2Tb]^-[TBA]^+ \times 3$ [TBA]Br $\times$ 3 H_2O with the compound crystallizing in the monoclinic space group $P2_1/c$ and four formula units in the unit cell (Figure 2A). Note that not all excess [TBA]Br molecules were trapped in the crystalline material. The TBAs cation and the $[Pc_2Tb]^-$ anion alternate in stacks along the *b*-axis. Here, the trough-space metal-to-metal distance is considerably large, d(Tb−Tb) = 22.95−23.24 Å. Along the *c*-axis, zigzag chains evolve with closer and alternating distances among neighboring Tb^{3+} ions (13.08 Å and 12.35 Å). Such arrangement gives short −CH···HC− contacts, potentially magnetic, between neighboring *Pc* molecules (C···C contacts between 2.829 Å and 2.774 Å). Because the $[TBA]^+$, Br^-, and solvent molecules preferentially locate themselves in alternate stacks with respect to $[Pc_2Tb]^-$, as also observed in the other crystal structure known for this compound (*vide infra*).[53] The addition of large excess of [TBA]Br should destabilize in the powder such −CH···HC− contacts witnessed along the crystallographic *c*-axis hindering the possible magnetic interaction between $[Pc_2Tb]^-$ neighboring molecules by increasing furthermore their segregation inside the matrix. The terbium (III) metal ion, as shown in Figure 2B, is coordinated by eight phthalocyanine nitrogens with an averaged Tb−N distance of 2.443 Å and adopts a square distorted antiprism as for the coordination polyhedron. The metal-ion displacement from the plane defined by the coordinating isoindole nitrogens N1A−N3A−N5A−N7A is 1.408 Å, and from the other plane defined by N1B−N3B−N5B−N7B is 1.420 Å. The resulting interplane distance of 2.828 Å between *Pc* rings is practically identical to the distance found for the compound $[Pc_2Tb]^-[TBA]^+ \times CH_3OH \times 3/2$ H_2O that exhibits, however, a different composition, crystal system, and also space group (orthorhombic, $Pna2_1$).[53] Collection of the structural parameters and solution refinements for $[Pc_2Tb]^-[TBA]^+ \times 3$ [TBA]Br $\times$ 3 H_2O are given together in Table 1.

Solid-State ^{1}H NMR Analyses of the $[Pc_2Tb]^-$ Units at Different Diamagnetic Dilution. The properties of SIMM are defined to a large extent by the intrinsic nature (electronic) of

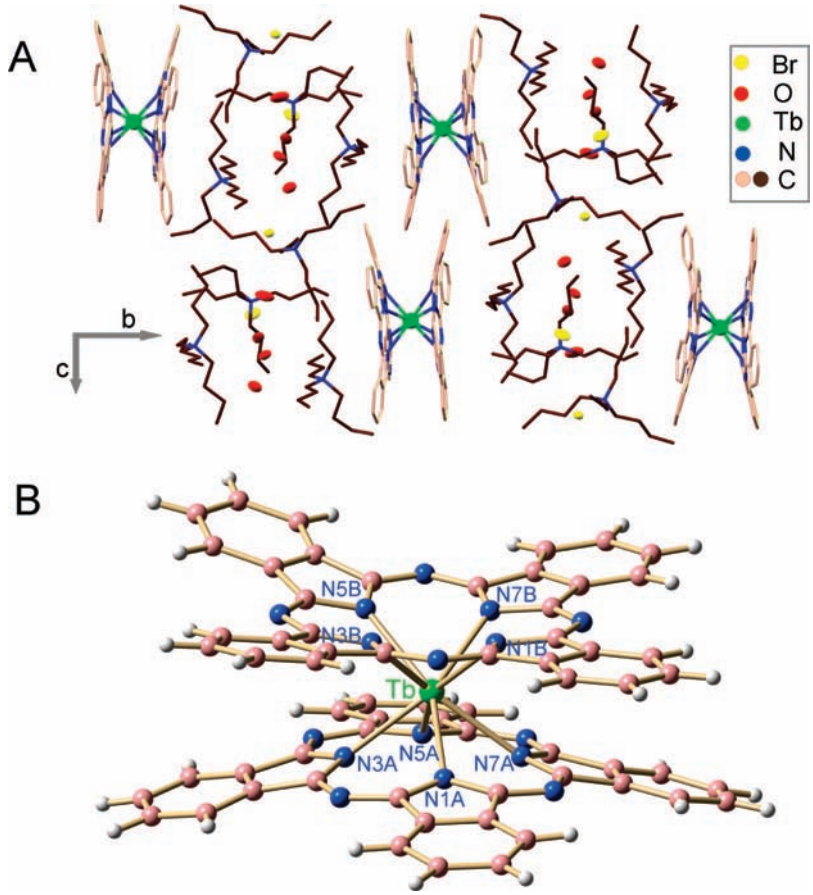

Figure 2. (A) Packing sketch of $[Pc_2Tb]^-[TBA]^+ \times 3$ [TBA]Br $\times 3$ H_2O (**4**), showing the allocation of the $[Pc_2Tb]^-$ complex anions in the unit cell. (B) Molecular structure of the $[Pc_2Tb]^-$ complex anion in **4** showing the Tb^{3+} metal ion (green) coordinated by the phthalocyaninato ligands (carbons: pink; hydrogen: gray; nitrogens: blue). Relevant Tb−N (intramolecular) distances: Tb(1)−N(1A), 2.548(6) Å; Tb(1)−N(3A), 2.340(5) Å; Tb(1)−N(5A), 2.509(6) Å; Tb(1)−N(7A), 2.357(5) Å; Tb(1)−N(1B), 2.535(6) Å; Tb(1)−N(3B), 2.313(5) Å; Tb(1)−N(5B), 2.573(6) Å; Tb(1)−N(7B), 2.338(6) Å.

Table 1. X-ray Data for $[Pc_2Tb]^-[TBA]^+ \times 3$ [TBA]Br $\times 3$ H_2O (**4**), Experimental Details, Structure Solutions, and Refinements

empirical formula	$C_{128}H_{182}Br_3N_{20}O_3Tb$
formula weight	2447.59
temperature	120(2) K
wavelength	0.34250 Å
crystal system, space group	monoclinic, $P2_1/c$
unit cell dimensions	$a = 13.807(2)$ Å
	$b = 37.015(5)$ Å
	$c = 25.127(5)$ Å
	$\alpha = 90°$; $\beta = 100.764(9)°$; $\gamma = 90°$
volume	12616(3) Å^3
Z, calculated density	4, 1.289 Mg/m^3
absorption coefficient	0.846 mm^{-1}
$F(000)$	5136
crystal size, color	0.12 mm × 0.11 mm × 0.07 mm, blue
θ range for data collection	$1.01° \le \theta \le 10.97°$
limiting indices	$-15 \le h \le 15$, $-41 \le k \le 41$
	$-27 \le l \le 27$
reflections collected/unique	64949/17144 [R(int) = 0.1127]
completeness to θ	94.6%
refinement method	full-matrix least-squares on F^2
data/restraints/parameters	17144/9/1415
reflections with $I > 2\sigma(I)$	11177
Extinction coefficient	0.0048(5)
largest diff. peak and hole	1.621 and −1.031 e·A^{-3}
goodness-of-fit on F^2	1.030
final R indices [$I > 2\sigma(I)$]	R1 = 0.0679, wR2 = 0.1569
R indices (all data)	R1 = 0.1136, wR2 = 0.1753

the individual molecule. However, strong evidence in recent years has demonstrated that, within the lattice, the molecules are not always magnetically identical and nearby molecules can interact via exchange forces with one another.[31] Distribution in magnetic properties can produce either small effects or can be quite remarkable. This is seen, for example, in the quantum tunneling of magnetization that can be switched on and off with small applied fields or through exchange interactions with neighboring molecules.[29] In order to explore the influence of the molecular surrounding on the spin dynamic of the terbium (III) metal ion, solid-state ^{1}H NMR measurements were performed on a series of batches made by differently diamagnetically diluted samples, $[Pc_2Tb]^-[TBA]^+$ (**1**), $[Pc_2Tb]^-[TBA]^+ \times 9$ [TBA]Br (**2**), and $[Pc_2Tb]^-[TBA]^+ \times 143$ [TBA]Br (**3**). The ^{1}H NMR spectra for the diluted samples **2** and **3** exhibit a progressive line broadening upon cooling (Figure 3A), featuring a Gaussian line-shape below 200 K. Above room temperature, however, the line changes to Lorentzian-like, and a narrow component grows on top of a broader one with intensity increasing upon increasing the sample temperature. A very different behavior characterizes the undiluted sample $[Pc_2Tb]^-[TBA]^+$ (**1**). Here, the ^{1}H NMR spectra could be recorded only over a limited temperature range, precisely only below 40 K and over 100 K, because the fast proton relaxation occurring in the range $40\ K < T < 100\ K$ prevented observation of the NMR signals. Above 100 K and up to room temperature, the signal line-shape remains Gaussian. On the contrary, upon decreasing the temperature to cryogenics, the ^{1}H NMR spectrum in **1** becomes very broad (Figure 3B), which indicates that in $[Pc_2Tb]^-[TBA]^+$ the average hyperfine coupling with the

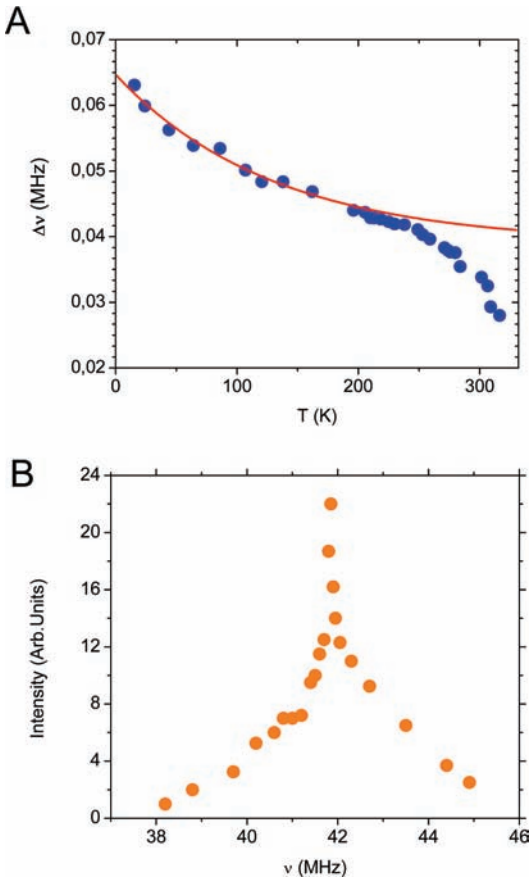

Figure 3. (A) Temperature dependence of ^{1}H NMR line width in $[Pc_2Tb]^-[TBA]^+ \times 9$ [TBA]Br (**2**) and $[Pc_2Tb]^-[TBA]^+ \times 143$ [TBA]Br (**3**). The solid line shows the behavior expected from the temperature dependence of the susceptibility (χ_{mol}) as reported in eq 2. A clear narrowing is evident above 200 K. (B) ^{1}H NMR spectrum of $[Pc_2Tb]^-[TBA]^+$ (**1**) recorded at $T = 21$ K, showing the very broad line width.

protons is much larger than in the more diluted samples **2** and **3**. The broad spectrum provides direct evidence that the Tb^{3+} magnetic moments are frozen already at 20 K and fluctuate at frequencies well below the MHz range. The nuclear spin−lattice relaxation rates were extracted for **1**, **2**, and **3** from the recovery of nuclear magnetization $m(\tau)$, after a saturation recovery pulse sequence. Below 200 K the recovery law $y(\tau) = 1 - m(\tau)/m(\tau\rightarrow\infty)$ behaves as a stretched exponential function (see eq 1) irrespective of the diamagnetic [TBA]Br dilution employed.

$$y(\tau) = \exp(-(\tau/T_1))^{\beta} \qquad (1)$$

In **2** and **3** the values of the exponent (β) were found to be $\cong$0.5 and almost temperature independent, while in **1** the value of β was close to unity. Such expression for the recovery law mirrors the presence of a distribution in relaxation rates for different ^{1}H nuclei arising from the different hyperfine couplings between ^{1}H nuclei and Tb^{3+} ions. Accordingly, the spin−lattice relaxation rate $1/T_1$ obtained by fitting the recovery with eq 1 provides an averaged value over the whole distribution. The observed temperature dependence of $1/T_1$ for **2** and **3** initially showed poor reproducibility. In fact, the relaxation rates $1/T_1$, are found to be functions of both the cooling rate and the intensity of the magnetic field applied within cooling procedures. Trials were made in order to optimize the experimental conditions which granted reproducibility later on. These conditions were obtained by annealing the diluted samples for 30 min at 320 K and then cooling down to 200 K at a rate of 1 K min^{-1} or less) under 1 T of applied magnetic field. The $1/T_1$ temperature dependence results for **3** and **2**, recorded below $T = 200$ K after employment of such annealing and cooling procedures, are depicted in Figure 4A and 4B, respectively. Both samples evidenced the presence of a peak in $1/T_1$ around 130 K, while at lower temperatures the $1/T_1$ trends versus T produced a strained shoulder. Furthermore, the intensities of the high-temperature peaks were found inversely proportional to the field intensity (Figure 4C). These properties highlight the presence of fluctuations at a frequency ν close to the nuclear Larmor frequency (ν_0). On the contrary, in $[Pc_2Tb]^-[TBA]^+$ (**1**), $1/T_1$ was unaffected by the cooling rate and the intensity of the

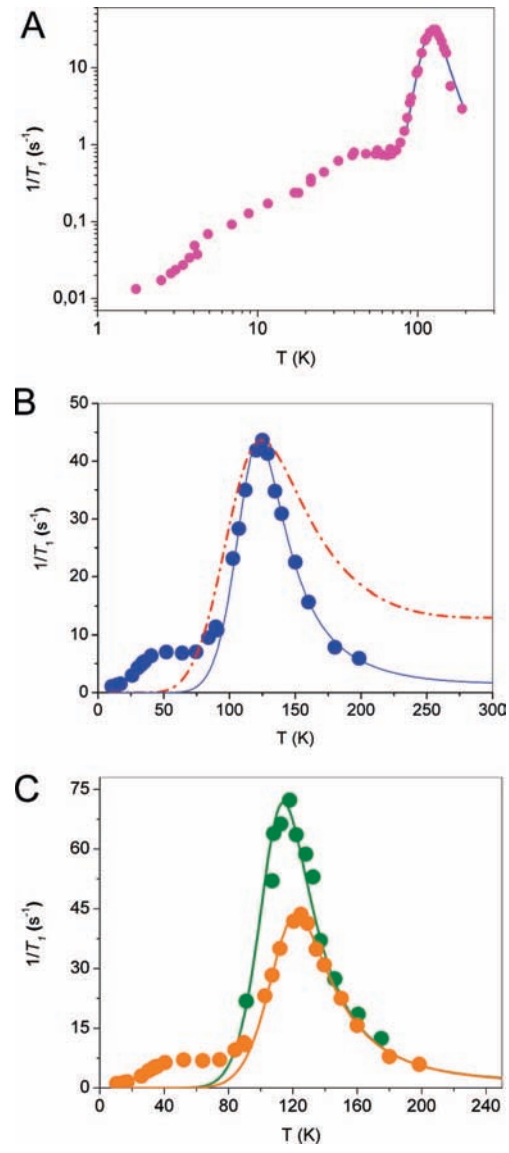

Figure 4. (A) Temperature dependence of $1/T_1$ in $[Pc_2Tb]^-[TBA]^+ \times 143$ [TBA]Br (**3**) powders for $H_0 = 4.5$ kG. The solid circles are experimental data. The solid blue-line in the high-temperature range represents the best fit according to eq 10) (see text). (B) Temperature dependence (circle) of $1/T_1$ in $[Pc_2Tb]^-[TBA]^+ \times 9$ [TBA]Br (**2**) powders for 4.5 kG of applied field. The dashed−dotted red line shows the behavior expected according to eq 4 and assuming the sublevel scheme proposed by Ishikawa et al. (see main text)[40,58] and the blue solid line the fitting result according to eq 8. (C) Field and temperature dependence of $1/T_1$ in $[Pc_2Tb]^-[TBA]^+ \times 9$ [TBA]Br (**2**) powders for $H_0 = 4.5$ kG (green circles) and $H_0 = 2.7$ kG (orange circles). The solid lines (green and orange) show again the best fit according to eq 8.

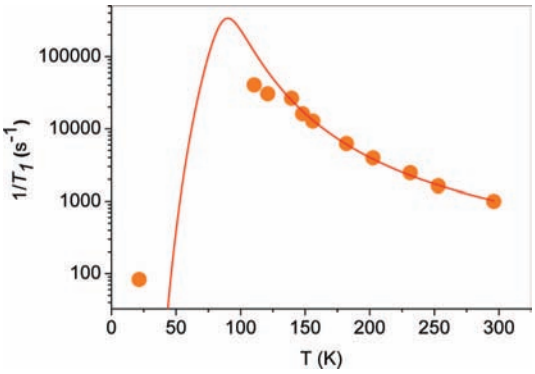

Figure 5. Temperature dependence of ^{1}H $1/T_1$ in $[Pc_2Tb]^-[TBA]^+$ (**1**) powders (solid circle) under an applied magnetic field of 1 T. The solid line shows the temperature dependence of $1/T_1$ expected with eq 8 (see the main text) for an energy barrier ΔE of 841 K (584 cm^{-1}).

magnetic field applied while cooling, which evidenced no history dependence. From these results it is evident that excess of $[TBA]^+$ and its molecular arrangement around $[Pc_2Tb]^-$ can significantly affect $1/T_1$. We furthermore remark that in the undiluted sample **1**, $1/T_1$ is more than 2 orders of magnitude larger than in **2** and **3**, as shown in Figure 5, and below 100 K the relaxation is so fast that makes impossible to detect the proton signal, which is recovered only below 40 K when also the transverse relaxation time becomes again long enough. The detailed analysis of the ^{1}H NMR line-width ($\Delta\nu$) and $1/T_1$ can provide further insight on the rotational dynamics of $[TBA]^+$ and its potential effect on tuning the relaxation barrier of $[Pc_2Tb]^-$. The theoretical treatment is presented in the following section.

The ^{1}H NMR Line Width Analyses of $[Pc_2Tb]^-$ in Different Diamagnetic Dilution. At low temperature the line width $\Delta\nu$ progressively increases upon cooling in a way proportional to the spin susceptibility χ_{mol} (Figure 3A and 3B). In each unit cell of **2** and **3** several protons are present, each of them characterized by a different hyperfine coupling with Tb^{3+} ions and by different paramagnetic shifts, given by eq 2

$$K = \frac{A\chi_{mol}}{2\mu_B N_A} \tag{2}$$

Here, the factor A represents the hyperfine coupling tensor and χ_{mol} the molar susceptibility. Any distribution in A would therefore cause a spread of paramagnetic shifts, ΔK, and a broadening proportional to the magnetic susceptibility χ_{mol}. Moreover, in a powder sample, depending on the orientation of each crystallite with respect to the magnetic field, different components of the paramagnetic shift tensor are sensed simultaneously. Hence, the spectra for **2** and **3** are characterized by broadening associated also with the angular distribution of the paramagnetic shifts. In addition to that, it has been found that in $\Delta\nu/\nu_0 \propto \Delta K$ the proportionality factor includes several terms such as the angular and site dependence of the hyperfine couplings and the anisotropy of the susceptibility itself. Therefore, from the observed line width data, it is possible to give only an estimate of the order of magnitude of the hyperfine coupling, which falls in the range of a few tens of Gauss. Such estimate is consistent with a hyperfine coupling dominated by the dipolar term. It should be remarked that in **2** and **3** most of the ^{1}H nuclei belong to the TBA molecules, and thus they are located rather apart from the the Tb^{3+} metal ions. In undiluted **1**, where most of the NMR signal comes from ^{1}H nuclei within *Pc* molecules, a much larger average hyperfine coupling was observed. In fact, at low temperature a significant broadening of the line emerges (Figure 3B) consistent with a hyperfine field of about 500 Gauss. At high temperature, $\Delta\nu/\nu_0$ is no longer proportional to χ_{mol} in **2** and **3** (Figure 3A). The observed breakdown of the linear trend originates from the onset of the molecular motions. Then, above room temperature, the onset of a narrow component in the ^{1}H NMR spectrum can be observed together with the progressive disappearance of the broader part of the spectrum. The narrowing of the line can be associated with the fast rotational dynamics of $[TBA]^+$ molecules at a frequency ν larger than the rigid lattice line width measured at lower temperatures. The insurgence of a narrow component on top of a broader one for both diluted samples **2** and **3** indicates that the molecular dynamics are not characterized by a single correlation time but rather by a distribution of them. As the temperatures were raised, more and more molecules reach the motional narrowing conditions, and the intensity of the narrow component in the NMR spectra increases. The line width analyses indicate that all these processes are frozen below 200 K and therefore irrelevant in the analysis of $1/T_1$ data. Analyses of the spin dynamic trends are then presented in the following part. The different configuration in which the $[TBA]^+$ cation freezes below 200 K is therefore expected to affect the crystal field and accordingly the spin dynamics of these systems.

Spin Dynamics in $[Pc_2Tb]^-$ Derived from $1/T_1$. The determination of ^{1}H nuclear spin−lattice relaxation rate allows to probe the low frequency fluctuations of Tb^{3+} moments at the microscopic level, caused by the transitions among the different crystal field states. In the framework of the weak collision approximation, the ^{1}H nuclear spin−lattice relaxation rate can be expressed according to eq 3

$$\frac{1}{T_1} = \frac{\gamma^2}{2}\int e^{i\omega_0 t}\langle h_+(t)h_-(0)\rangle dt \tag{3}$$

where γ indicates the proton gyromagnetic ratio and $h_\pm$ are the components of the hyperfine field at the nucleus perpendicular to the external magnetic field orientation. In view of the energy difference between the hyperfine levels and the m levels of Tb^{3+}, the direct nuclear relaxation process involving a spin excitation is forbidden. The effective relaxation processes are indirect ones, thus involving a nuclear spin flip without change in m. This is possible as the dipolar hyperfine Hamiltonian contains terms coupling $h_{x,y}$ to J_z. Upon considering that each crystal field level m is characterized by a finite lifetime (τ_m) due to spin−phonon scattering processes, and upon taking a Lorentzian broadening of the sublevels, $1/T_1$ can be rationalized through use of eq 4,[59]

$$\frac{1}{T_1} = \frac{\gamma^2 < \Delta h_\perp^2 >}{Z}\sum_{m=-6}^{m=+6}\frac{\exp(-E_m/k_B T)\tau_m}{1+\omega_0^2\tau_m^2} \tag{4}$$

where the term $<\Delta h_\perp^2>$ indicates the mean-square amplitude of the hyperfine field fluctuations, E_m the eigenvalues of the crystal field levels, and Z the corresponding partition function. The lifetime for the m sublevels can also be formulated in terms of the transition probability $p_{m,m\pm1}$ between m and $m \pm 1$ states according to eq 5.

$$\frac{1}{\tau_m} = p_{m,m-1} + p_{m,m+1} \tag{5}$$

Since the life-times are mainly determined by spin−phonon scattering processes, those can be expressed in terms of eigenvalues of the crystal field levels with eqs 6 and 7,[59]

$$p_{m,m+1} = C\frac{(E_m - E_{m+1})^3}{1 - (\exp(E_{m+1} - E_m)/k_BT)} \quad (6)$$

$$\frac{1}{T_1} = \frac{\gamma^2 < \Delta h_\perp^2 >}{2} \times \frac{2\tau_c}{1 + \omega_0^2\tau_c^2} \quad (7)$$

where C represents the spin−phonon coupling term. Upon taking the sublevel scheme proposed earlier in the literature,[39] the expected temperature dependence of $1/T_1$ was derived from eq 4 where two adjustable parameters $<\Delta h_\perp^2>$ and the constant C have been considered. The results are shown in Figure 4B. It is evident from the trend that the observed $1/T_1$ behavior against T is not well reproduced. On the other hand, the high temperature peak in $1/T_1$ could be nicely reproduced by considering that the correlation function for the hyperfine field fluctuations is described by a single correlation time. This would imply that, within the explored temperature range and below 200 K, actually just the lowest levels are occupied. In this case, by considering that in the range $100 \leq T \leq 200$ K the thermal energy is much larger than the splitting between the $m = \pm 6$ levels, these two levels can be considered degenerate, and eq 5 simplifies into eqs 8 and 9.

$$\frac{1}{T_1} = \frac{\gamma^2 < \Delta h_\perp^2 >}{2} \times \frac{2\tau_c}{1 + \omega_0^2\tau_c^2} \quad (8)$$

$$\tau_c = (C\Delta E^3)^{-1} \times [\exp(\Delta E/k_BT)] \quad (9)$$

with ΔE the energy difference between the $m = \pm 6$ and $m = \pm 5$ doublets. The best fit of the experimental data through the use of eqs 8 and 9 yields C about 260 Hz/K^3 and a splitting $\Delta E \cong 923$ K (e.g., $\Delta E \cong 641$ cm^{-1}). This splitting is much larger than the one derived by Ishikawa et al.[40,58] and significantly larger than the anisotropy barrier of any other known single molecular magnet. It should be noticed that in this system the coupling constant C is about 2 orders of magnitude smaller than the one of Mn_{12}.[59] In the case of **1** for $<\Delta h_\perp^2> \cong (500)^2$ Gauss^2, as estimated from the low-temperature NMR spectra (see Figure 3B), the experimental data were nicely reproduced with $\Delta E \cong$ 840 K (e.g., $\Delta E \cong 584$ cm^{-1}) and a constant C $\cong$ 5000 Hz/K^3 (Figure 5). The results indicate that in **1** the spin−phonon coupling is very large and yields to a very short lifetime of crystal field levels, i.e. the system had a fast dynamics. Although we could not measure $1/T_1$ close to the expected peak position (around 80 K) owing to the extremely fast nuclear spin-relaxation rates, it is worth mentioning that recent μSR measurements[63] showed that the muon (μ) $1/T_1$ exhibits a peak around 80 K, in full agreement with these findings. Below 80 K a clear departure is observed from the behavior expected on the basis of an activated form for τ_c. For $k_BT \ll \Delta E$ the lifetime of the ground-state doublet is determined only by the transitions among the $m = +6$ and -6 states. Therefore, this transition probability is determined by the mixing of the $|m>$ states, which is sizeably affected by the crystal field symmetry and thus by the arrangement of $[TBA]^+$ molecules around $[Pc_2Tb]^-$. These transitions yield a nearly temperature-independent $1/T_1$ between

(63) Branzoli, F. Unpublished work.

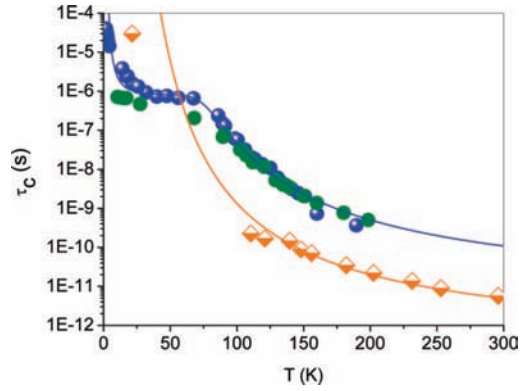

Figure 6. Temperature dependence of the characteristic fluctuation times for $[Pc_2Tb]^-$ magnetic moment as derived from $1/T_1$ data. The blue circles represent experimental data for $[Pc_2Tb]^-[TBA]^+ \times 143$ [TBA]Br (**3**), and the green circles, those for $[Pc_2Tb]^-[TBA]^+ \times 9$ [TBA]Br (**2**). The solid blue line shows the best fit to the $[Pc_2Tb]^-[TBA]^+ \times 9$ [TBA]Br (**2**) data according to eqs 10−12. The diamonds show the $[Pc_2Tb]^-[TBA]^+$ (**1**) experimental data. The orange line represents the corresponding activated high-temperature contribution to the relaxation time.

80 and 30 K. At lower temperatures, when $k_BT \leq 12g\mu_BH_0$, the Zeeman splitting among the $m = \pm 6$ levels prevents the tunneling processes and the mechanism becomes activated again with an energy gap Δ_H related to the Zeeman splitting. In order to derive the temperature dependence of the correlation time describing the Tb^{3+} moments fluctuations, it is necessary at first to calculate $<\Delta h_\perp^2>$ from the amplitude of the $1/T_1$ peaks and then, starting from eq 8 and from the experimentally determined $1/T_1$, to derive the correlation time τ_c. The temperature dependences of τ_c for the three samples, hence **1** undiluted, **2** and **3** diluted molecules, are reported in Figure 6. In the case of **2** and **3**, the τ_c terms show at high temperatures practically the same T dependency, irrespective of their different diamagnetic dilution, with the activated trend mentioned in the previous paragraph. As for **1**, on the other hand, the τ_c was much shorter. This effect is due to the smaller energy barrier characterizing **1** and to the larger spin−phonon coupling constant. Below 80 K a plateau is present, and the estimated value for τ_c in (**3**) is larger than the one observed in (**2**). This variation should be ascribed to the different tunneling rate characterizing the systems, which can be associated with a different symmetry of the crystal field around $[Pc_2Tb]^-$ and to a different state mixing in the two differently magnetically diluted samples. Below 30 K, the activated increase of τ_c, associated with the Zeeman splitting, is finally detected. The total correlation time for the hyperfine field fluctuations can be expressed in the form of eq 10 in terms of both the high-temperature activated contribution (eqs 4−8) and the tunneling processes among ± 6 states.

$$\frac{1}{\tau_c} = \left(\frac{1}{\tau_c}\right)_{act} + \left(\frac{1}{\tau_c}\right)_{tun} \quad (10)$$

where $(1/\tau_c)_{tun}$ is practically temperature independent when $k_BT > 12g\mu_BH_0$. It should be noticed that in a powder sample the Zeeman splitting would depend on the orientation of the magnetic field with respect to the anisotropy axes z. In fact, one can write $\Delta_H = 12g\mu_BH_0 \cos\theta$, with θ the angle between $\vec{H}_0$ and $\hat{z}$. Accordingly, the correlation time estimated in the low-temperature range corresponds to an average over all possible orientations of τ_c, and thus it is possible to derive eqs 11 and 12.

$$(\tau_c)_{tun}(T) = (\tau_c)_{tun}(\infty) \int_0^{\pi} \sin\theta \times \exp(12g\mu_B H_0 \cos\theta/k_B T)\mathrm{d}\theta \quad (11)$$

$$(\tau_c)_{tun}(T) = (\tau_c)_{tun}(\infty) \sinh\left(\frac{12g\mu_B H_0 \cos\theta}{k_B T}\right)/\left(\frac{12g\mu_B H_0 \cos\theta}{k_B T}\right) \quad (12)$$

Here, $(\tau_c)_{tun}(\infty)$ represents the correlation time at temperatures $T >> \Delta_H/k_B$. The experimentally determined τ_c values reported in Figure 6 can be modeled through eq 10 taking for $(\tau_c)_{tun}$ the expression given in eqs 11 and 12. While the analysis provides satisfactory fitting of the data down to ~20 K, at lower temperature eqs 11 and 12 fail to describe exactly the temperature dependence of the correlation time. This discrepancy between theory and experimental findings can be tentatively explained at present by partial orientation of $[Pc_2Tb]^-$ molecules during the cooling procedure.

Conclusion

In this work we describe the synthesis of a series of bis-phthalocyaninato terbium (III) compounds **1**, **2**, and **3**, where the magnetically active $[Pc_2Tb]^-$ anions were diluted through the use of the diamagnetic TBA^+Br^- matrix material. Exemplarily, the molecular structure of one of the TBA^+Br^- matrix diluted compounds, $[Pc_2Tb]^-[TBA]^+ \times 3$ $([TBA]^+Br^-) \times 3$ H_2O (**4**), could be solved by single-crystal X-ray diffraction studies elucidating the structural consequences brought by magnetic dilution. The spin dynamics of the *f*-metal ion was then probed by solid-state ^1H NMR techniques. The energy barrier was found much larger (584 cm^{-1} −641 cm^{-1}) with respect to those previously estimated for the $[Pc_2Tb]^-[TBA]^+$ system (~230 cm^{-1})[40,58] and even one order of magnitude larger than in any other SMM system.[37] Moreover, it could be shown that the barrier height and tunneling rates depend on the magnetic dilution employed. The spin dynamics of the diamagnetically diluted $[TbPc_2]^-$ molecules in the samples **2** and **3** were affected by their magneto/thermal history, suggesting that even the diamagnetic matrix arrangement around $[Pc_2Tb]^-$ can perturb the splitting of the crystal field levels. The small discrepancy between theory and experimental results observed in the Tb^{3+} spin dynamics at low temperature (<20 K) emphasizes the need of further progress in fundamental knowledge as a prerequisite for the effective application of these SIMM units in operational magnetic device elements.[60−62]

Experimental Section

All reagents (*n*-hexanol, 1,2-dicyanobenzene, 1,8-diazabicyclo[5.4.0]-undec-7-ene (DBU), terbium(III)-acetate, benzyl-triethylamonium chloride) were purchased from commercial sources and used as received. The synthesis of $[Pc_2Tb]^-[TBA]^+$ was carried out by employing several modifications of the general protocol based on the published procedure of Weiss and coauthors.[46] The preparative description for the diamagnetically diluted $[Pc_2Tb]^-[TBA]^+$ powders are reported in the synthetic section. The $[Pc_2Tb]^-[TBA]^+$ samples (~70−90 mg) were transferred under nitrogen inside 3−3.5 cm length NMR tubes, and then the tubes were sealed, avoiding sample heating. FT-IR spectrum was recorded on a Perkin-Elmer Spectrum GX spectrometer in KBr pellet at rt. UV−vis/nIR spectra were measured on Varian Cary 500 scan UV−vis/nIR spectrophotometer by using 1 cm optical path length quartz cell. Maldi-ToF spectra were recorded on Perseptive Biosystems Voyager-DePro using ferulic acid as matrix and 2,5-dihydroxybenzoic acid or 3-hydroxypicolinic acid as calibration matrixes. The elemental analyses were obtained with a Vario Micro Cube apparatus and metal content (terbium) by induced coupled plasma spectroscopy (ICP). Solution paramagnetic ^1H NMR spectra were recorded at 298 K on a Bruker 300 Ultrashield spectrometer. Solid-state ^1H NMR measurements were carried out using standard radiofrequency pulse sequences. The spectra were obtained from the Fourier transform of half of the echo signal after a $\pi/2-\pi-\pi$ pulse sequence. Magnetic measurements were carried out with a Quantum Design (SQUID) Magnetometer MPMS-XL-5. The susceptibility data were corrected for the diamagnetic contributions calculated using the Pascal constants. DC data were collected with an applied field of 1000 G (10^{-4} T) in the 2−300 K temperature range. AC data were collected in the 2−60 K range with an applied alternating field of 3.95 G (0.395×10^{-3} T) at different frequencies in the 1−997 Hz range. The crystallographic data were collected at the ESRF Synchrotron Facility (Grenoble, France) at the beam line No. 11. The structures were solved by direct methods (SHELX-97). Refinement was performed with anisotropic temperature factors for all non-hydrogen atoms (disordered atoms were refined isotropically).

Preparation of Bis(phthalocyaninato)terbium(III)tetrabutylamonium ($[Pc2Tb]^-[TBA]^+$) (1). In a round-bottomed flask were mixed dicyanobenzene (32.0 mmol, 4.1 g), terbium acetoacetate (2.0 mmol, 0.64 g) in hexanol (50 mL), DBU (16.0 mmol, 2.4 mL), and a catalytic amount of benzyl-triethylamonium chloride (30 mg, 0.13 mmol). The reaction was performed in a microwave oven using an applied microwave power of 450 W for 10 min, followed by longer irradiation (15 min) at lower energy (300 W). The blue mixture was cooled down to rt and kept in the cold (4 °C) overnight. The dense solution was filtered using a glass frit and the residue collected. In order to remove as much *n*-hexanol as possible, the precipitate was further washed on frit with portions of cold *n*-heptane (5 × 50 mL). Then the products $[Pc_2Tb]^-$ (blue) and $[Pc_2Tb]^0$ neutral (green) were extracted from the residue, using a mixture of $MeOH/CH_2Cl_2$ (200 mL, 50 mL, 4 °C), while most of the phthalocyanine ring (violet, very shiny needles) remained in this way on the filter. The solution was evaporated to dryness under reduced pressure which afforded formation of an oily blue-green residue. Addition of CH_2Cl_2 (30 mL) followed by hexane (400 mL) allowed slow formation of a fine, bluish precipitate after 30 min that was collected while the yellow-greenish solution was filtered off. This procedure was repeated three times. Purification of $[Pc_2Tb]^-$ was performed by nitrogen-saturated flash chromatography on an Al_2O_3 (basic) column where at first CH_2Cl_2 was used as eluent to remove remaining yellowish side products followed by CH_2Cl_2/MeOH (2/1, v/v). The product $[Pc_2Tb]^-$ was then eluted by addition of sodium methanoate (NaOMe) using only MeOH as eluting solvent. The blue fraction collected was quickly evaporated to dryness under reduced pressure and kept under nitrogen. Further purification of $[Pc_2Tb]^-$ was carried out by size-exclusion chromatography using Sephadex LH20 with $MeOH/CH_2Cl_2$ as eluent mixture (1/1, v/v). Residual bluish compounds remained trapped in the column. The blue solution was quickly evaporated under reduced pressure, affording the negatively charged product in the form of a very hygroscopic dark-blue powder (0.56 g, 0.47 mmol, yield 6%) which still contained one solvent molecule (*n*-hexanol) and where most probably an acid/water molecule acted as countercation. Analytical data for the unstabilized anion $[Pc_2Tb]^-$: found C 59.53, H 4.28, N 15.87, O 9.06, Tb 11.25; calculated for $C_{64}H_{32}N_{16}Tb \times$ *n*-hexanol $\times$ 7 H_2O: C 59.39, H 4.30, N 15.90, O 9.39, Tb 11.30. Tetrabutylammonium bromide (0.47 mmol, 0.153 g) was added to the blue solid $[Pc_2Tb]^-$ together with 50 mL of MeOH; the resulting deep-blue solution was then stirred vigorously under nitrogen for 5 min. Most of the solvent (~45 mL) was removed under vacuum, and cold hexane was added (100 mL). A dark-blue precipitate immediately formed, which was collected and dried in vacuum (0.1 mbar) at rt for one day and then stored under nitrogen (664 mg). The bulk magnetic properties of this sample were measured and found to be analogous to those already described by Ishikawa and co-workers (see Supporting Information).[40]

Analytical data for $[Pc_2Tb]^-[TBA]^+$: found C 66.64, H 4.82, N 16.33, O 1.33, Tb 10.87, Br traces (<0.1); calculated for $(C_{64}H_{32}N_{16}Tb) \times (C_{16}H_{36}N) \times H_2O$: C 66.52, H 4.88, N 16.48, O 1.11, Tb 11.00. IR (KBr pellet, ν/cm^{-1}): 3047 (w), 2989 (m), 2959 (s), 2873 (s), 1607 (m), 1474 (vs), 1405 (m), 1380 (m), 1329 (s), 1282 (m), 1162 (m), 1112 (s), 1079 (s), 1060 (s), 883 (s), 728 (s). UV/vis (MeOH, λ/nm, [ε ($M^{-1} \times cm^{-1}$)]): 674 (8.62×10^4), 623 (2.07×10^4), 336 (4.10×10^4). Paramagnetic ^{1}H NMR (CD_3CN), δ/ppm: −39.9 (br, H_β), −82.3 (br, H_α). Maldi-ToF (calibration matrix 2,5-dihydroxybenzoic acid) negative polarity mode: found: $m/z^- = 1183.22$ (100%, M^-), calculated for $C_{64}H_{32}N_{16}Tb$: $m/z^- = 1183.29$ (100%, M^-). Maldi-ToF (high-resolution) isotopic distribution pattern (calibration matrix: 3-hydroxypicolinic acid); found: $m/z^- = 1183.224$ (100%), 1184.227 (84%), 1185.230 (33%), 1186.233 (9%). The $[TBA]^+$ countercation was clearly detected once positive polarity mode was applied, but no detection was possible under negative polarity; Maldi-ToF (calibration matrix sinapinic acid) positive polarity mode, found: m/z^+ 241.87 (100%, M^+), calculated for $C_{16}H_{36}N^+$: $m/z^+ = 242.28$ (100%).

Preparation of Bis(phthalocyaninato)terbium(III)tetrabutylamonium Bromide [Pc2Tb]$^-$[TBA]$^+$ × 9[TBA]Br (2) and [Pc2Tb]$^-$[TBA]$^+$ × 143 [TBA]Br (3). Magnetically diluted $[Pc_2Tb]^-[TBA]^+$ samples were prepared by addition of tetrabutylamonium bromide salt solution as follows.

Preparation of ([Pc2Tb]$^-$[TBA]$^+$) × 9[TBA]Br (2). In a round-bottomed flask were mixed solid $[Pc_2Tb]^-[TBA]^+$ ($(C_{64}H_{32}N_{16}Tb) \times (C_{16}H_{36}N) \times H_2O$, 100 mg, 0.069 mmol) and a solution of tetrabutylammonium bromide in MeOH (201 mg, 0.623 mmol, 25 mL of MeOH). The mixture was stirred vigorously for 5 min followed by sonication of the solution in a water bath (5 min) at rt. Solvent evaporation under reduced pressure and high-vacuum drying (10^{-2} mbar, 70 °C) afforded a bluish powder in quantitative yield. Analytical data for $[Pc_2Tb]^-[TBA]^+ \times 9$[TBA]Br: found C 60.23, H 9.24, N 8.00, O 2.21; calculated for $(C_{64}H_{32}N_{16}Tb) \times (C_{16}H_{36}N)_{10}Br_9 \times 6\ H_2O$: C 60.41, H 9.19, N 8.18, O 2.51.

Preparation of ([Pc2Tb]$^-$[TBA]$^+$) × 143[TBA]Br (3). In a round-bottomed flask solid $[Pc_2Tb]^-[TBA]^+$ ($(C_{64}H_{32}N_{16}Tb) \times (C_{16}H_{36}N) \times H_2O$, 20 mg, 0.014 mmol) was mixed with a solution of tetrabutylammonium bromide in MeOH/CH_3CN (638 mg, 1.98 mmol, 100 mL MeOH/CH_3CN, 9/1, vol/vol). The so-formed mixture was stirred vigorously for 5 min, followed by sonication of the solution in a water bath (5 min) at rt. The solvent was evaporated under reduced pressure and then subjected to high-vacuum drying (10^{-2} mbar, 70 °C) which afforded a very pale bluish powder in quantitative yield. Analytical data for $[Pc_2Tb]^-[TBA]^+ \times 143$[TBA]Br: found C 59.26, H 11.23, N 4.55, O 0.53; calculated for $(C_{64}H_{32}N_{16}Tb) \times (C_{16}H_{36}N)_{144}Br_{143} \times 14\ H_2O$: C 59.51, H 11.06, N 4.69, O 0.50.

X-ray Analyses of $[Pc_2Tb]^-[TBA]^+ \times 3$ [TBA]Br $\times 3\ H_2O$ (4). Starting from the powder $[Pc_2Tb]^-[TBA]^+ \times 9$ [TBA]Br sample, suitable X-ray crystals of deep blue-violet color were grown in MeOH at 4 °C within one week by slow diffusion of diethylether. X-ray data for **4**, experimental details, structure solutions, and refinements are presented together in Table 1. The crystallographic data for the structure were deposited with the Cambridge Crystallographic Data Centre as supplementary publication, CCDC 705889.

Acknowledgment. M.R. and J.R.G.-M. thank the ERA-NET "Chemistry" project "MultiFUN" for kind support. The research activity in Valencia was also supported by the Spanish Ministerio de Educación y Ciencia (Projects CTQ2005-09385-C03-01 and CTQ2006-27186). The research activity in Pavia has been supported by CARIPLO2005 and CARIPLO 2008-2229 research funds. M.J.G. acknowledges support by the National Science Foundation "Materials World Network" through Grant DMR-0710525 and the Petroleum Research Fund of the American Chemical Society. The authors thank Dr. Gavin Vaughan from the ERSF Grenoble, Beamline 11, for collecting data for the X-ray diffraction experiment. G.Z. thanks the Research Council of Norway.

Supporting Information Available: Maldi-ToF spectra of $[Pc_2Tb]^-[TBA]^+$ (**1**) in the positive and negative polarity. The FT-IR spectrum of **1**. Magnetic susceptibility data (AC) of $[Pc_2Tb]^-[TBA]^+$ (**1**). The crystallographic file of **4** in CIF format. This material is available free of charge via the Internet at http://pubs.acs.org.

JA808649G